Supplementary Information

Tunable electrical properties of multilayer $HfSe_2$ field effect transistors by oxygen plasma treatment

Moonshik Kang,[a,b] Servin Rathi,[a] Inyeal Lee,[a] Lijun Li,[a] Muhammad Atif Khan,[a] Dongsuk Lim,[a] Yoontae Lee,[a] Jinwoo Park,[a] Sun Jin Yun,[c] Doo-Hyeb Youn,[c] Chungsam Jun[b] and Gil-Ho Kim*[a]

[a]College of Information and Communication Engineering and Sungkyunkwan Advanced Institute of Nanotechnology (SAINT), Sungkyunkwan University, Suwon 16419, Republic of Korea

[b]Manufacturing Engineering Team, Memory Division, Samsung Electronics Co., Hwasung 18448, Republic of Korea

[c]ICT Components and Materials Technology Research Division, Electronics and Telecommunications Research Institute, Daejeon 34129, Republic of Korea

*Corresponding author E-mail: ghkim@skku.edu

1. Degradation of electrical performance in $HfSe_2$ FETs without PR passivation

The requirement of photoresist (PR) passivation in the vicinity of the metal contacts in $HfSe_2$ FETs is illustrated in Fig. S1. If the devices are not treated for contact passivation, it results in the degradation of electrical performance (Fig. S1c and S1d) after O_2 plasma treatment. Besides the electrical degradation, the $HfSe_2$ layers were also damaged at the edge of the metal contacts, as seen from the optical images in Fig. S1a and S1b.

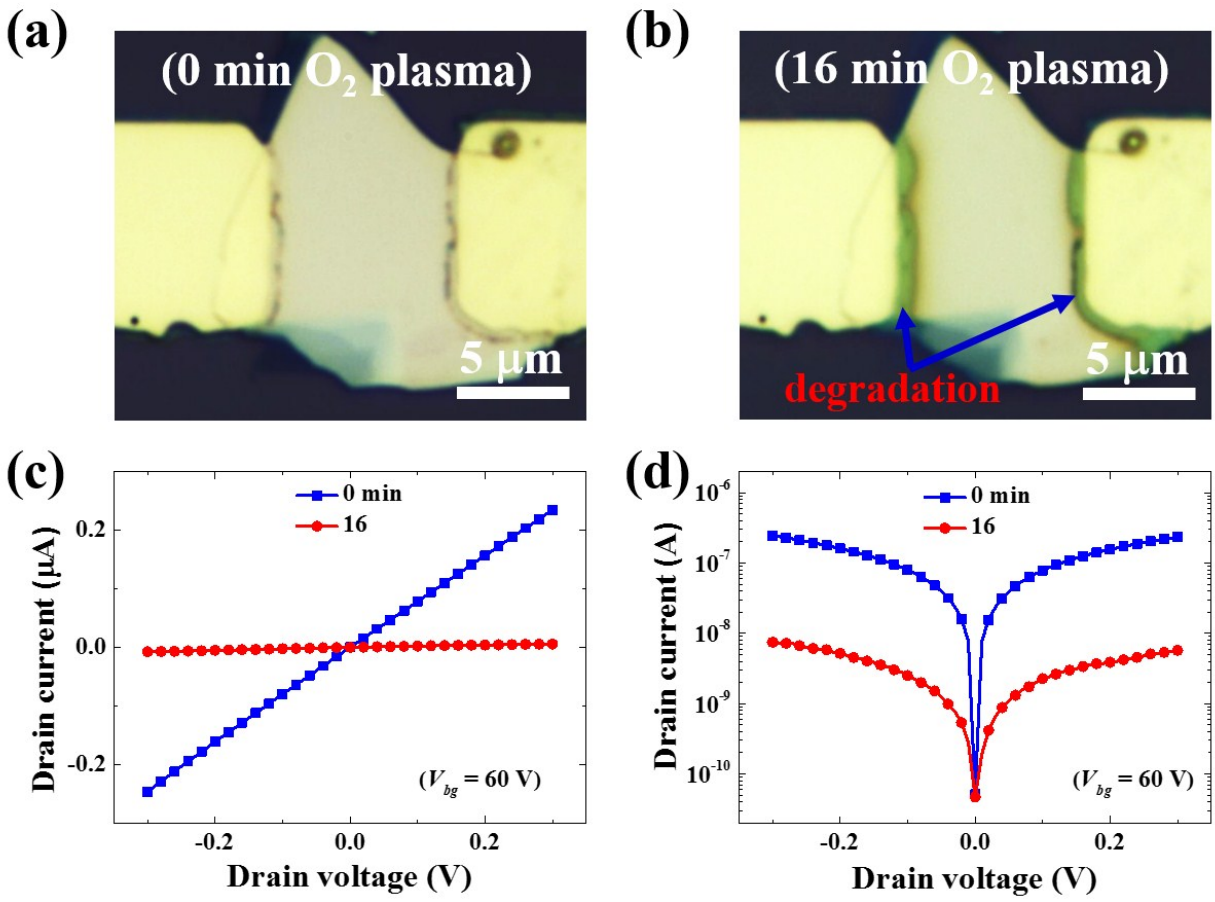

Fig. S1 Optical images of $HfSe_2$ FET (a) before and (b) after O_2 plasma treatment without the passivation of photoresist at the electrodes. The blue arrows indicate degradation at the metal electrodes. Output characteristics (I_{ds}-V_{ds}) of $HfSe_2$ FET before and after O_2 plasma treatment in (c) linear scale and (d) semi-logarithmic scale at room temperature, respectively.

The main reason behind the observed physical damage is joule heating at the non-ideal Ohmic contacts which enhances the oxidation of the layers at the contact regions. Therefore, the passivation of

the contact area by photoresist not only isolate them from oxidation in ambient conditions, but also protect the contact area from the O_2 plasma-induced oxidation.

2. Thickness-dependent Raman spectra of O_2 plasma-treated $HfSe_2$

The thickness dependent Raman spectra show that the thinner flakes have higher characteristic intensity of A_{1g} peak which decreases systematically with the flake thickness increase as shown in Fig. S2a. Whereas, after plasma treatment (50 W, 7 min), the HfO_x intensity peak (at 255 cm^{-1}) showed reverse trends, with the vanishing of A_{1g} peak for 4.5 nm flake, indicating the full transformation of the $HfSe_2$ into HfO_x. However, both A_{1g} and oxide peaks appeared for thicker flakes indicating a partial oxidation of the top layers which shield the bottom $HfSe_2$ layers and the exact number of top oxidized $HfSe_2$ layers depends on the given plasma power and time.

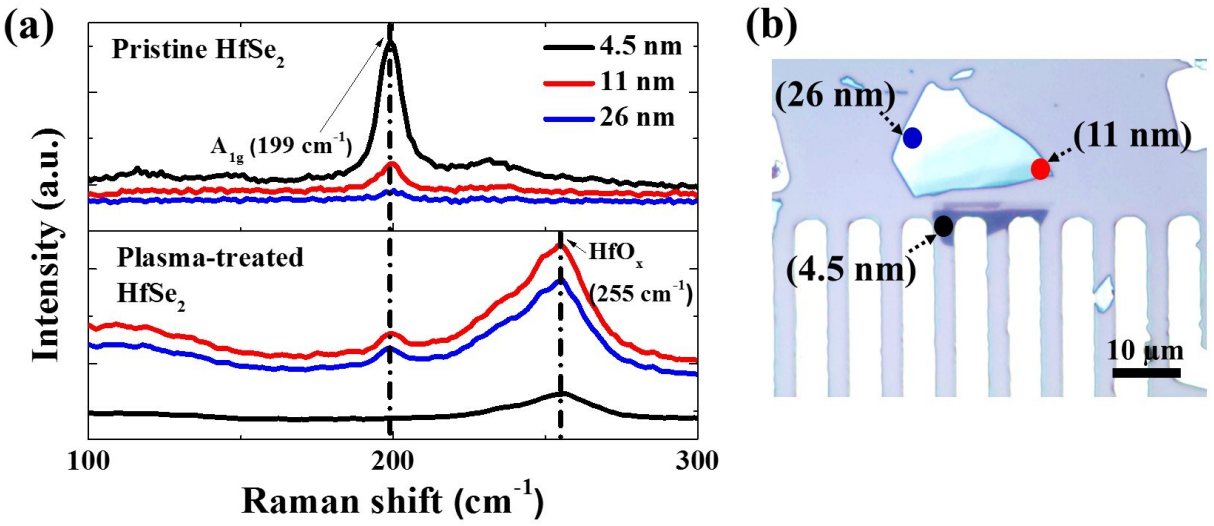

Fig. S2 (a) Raman spectra of 4.5, 11, and 26 nm thick $HfSe_2$ flakes represented by black, red, and blue color, respectively, for pristine and O_2 plasma-treated $HfSe_2$. (b) Optical image of the $HfSe_2$ flakes before the plasma treatment

3. Average increase in the thickness of $HfSe_2$ flake after O_2 plasma treatment

Fig. S3a shows the electrical characteristics of $HfSe_2$ FET with different O_2 plasma exposure times. The on/off ratio ($I_{on/off}$) increases by an order of magnitude from 10^2 to 3×10^3 and mobility (μ_{FE}) also

increases by 1.5 times of the initial value. Fig. S3b-d show that the plasma-treated $HfSe_2$ flake have higher roughness as compared to the photoresist covered layers. The increase in the thickness of plasma-treated $HfSe_2$ can be attributed to the expanded interlayer distance due to oxidation.

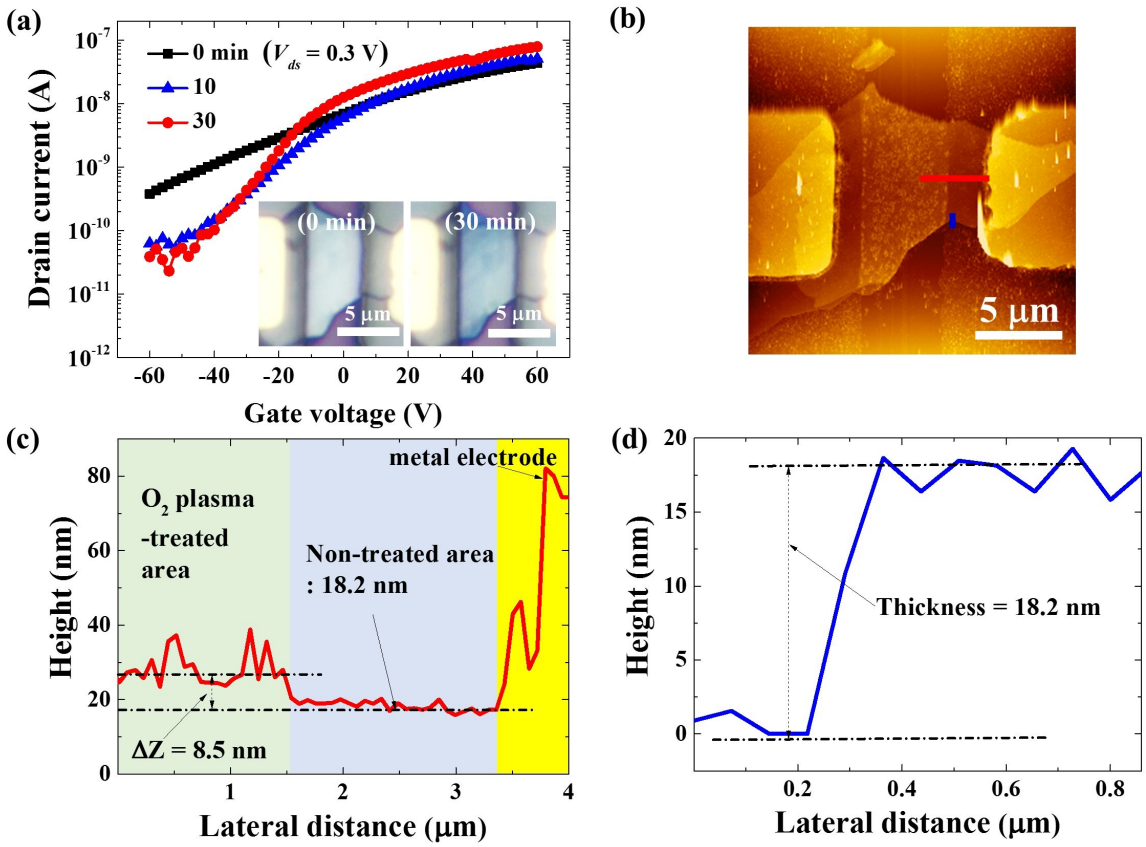

Fig. S3 (a) Transfer characteristics at V_{ds} = 0.3 V for $HfSe_2$ FET with different O_2 plasma exposure time, in semi-log scale. The insets show optical images of $HfSe_2$ FET before and after O_2 plasma treatment for 30 min. (b) AFM image, (c) thickness line-profile of the plasma-treated $HfSe_2$ along the red line, and (d) thickness line-profile (~ 18.2 nm) along the blue line of the photoresist covered $HfSe_2$. The average increase in the thickness of the O_2 plasma-treated $HfSe_2$ is approximately 8.5 nm.

4. Resistor network model for multilayer $HfSe_2$ back-gated FETs before and after O_2 plasma treatment

As discussed in the main manuscript that the thicker channel FETs are highly inefficient to turn off the device due to the screening effect of the bottom layers as the gate field is insufficient to deplete the top layers, thus resulting in a high off-current and poor device characteristic. The O_2 plasma treatment transform these top semiconducting layers to oxide layers which improves the device characteristics like on/off ratio ($I_{on/off}$) and subthreshold slope. The total resistance for the multilayer $HfSe_2$ devices is illustrated in Fig. S4a and S4b for pristine and O_2 plasma-treated devices. As seen from the figures that the pristine devices have high off-current whereas the O_2 plasma-treated devices are well controlled by the gate-field. Although, this lead to a slight drop in the on current of the device due to discontinuing of the parallel conduction in the top layers, but the on/off ratio ($I_{on/off}$) increases by several order of magnitude, thus resulting in the improved device performances.[S1,S2]

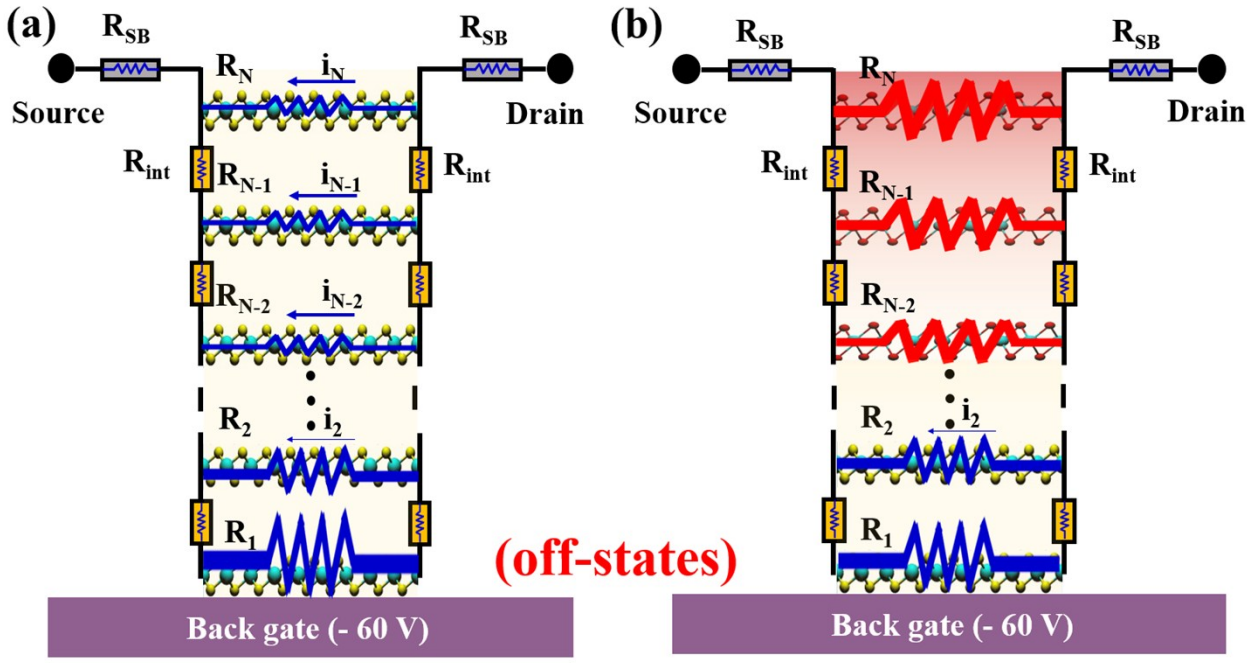

Fig. S4 Schematic diagrams for multi-layer $HfSe_2$ FETs (a) before and (b) after O_2 plasma treatment with resistor network models in the off-states. R_1 to R_N and i_2 to i_N are the intra-layer resistances and currents of each $HfSe_2$ monolayer, respectively. R_{int} is the interlayer resistance between two consecutive $HfSe_2$ layers, while R_{SB} is the contact resistance due to Schottky barrier height at the interface of metal and $HfSe_2$.

5. Transfer characteristics of O_2 plasma-treated $HfSe_2$ FETs with a thick channel at the various plasma power conditions

Fig. S5a-d show the effect of plasma treatment on very thick flakes (> 60 nm). As can be seen from the figures that even high plasma power treatment results in no improvements in the off-current. The possible reason for this behavior is that even after plasma treatment, the underlying $HfSe_2$ layers are still thick enough to screen the gate-field at the layer beneath the top oxidized layers by the plasma treatment. Therefore, this plasma process is only compatible to improve the performance of devices whose channel thickness lies in the range of ~10-20 nm.

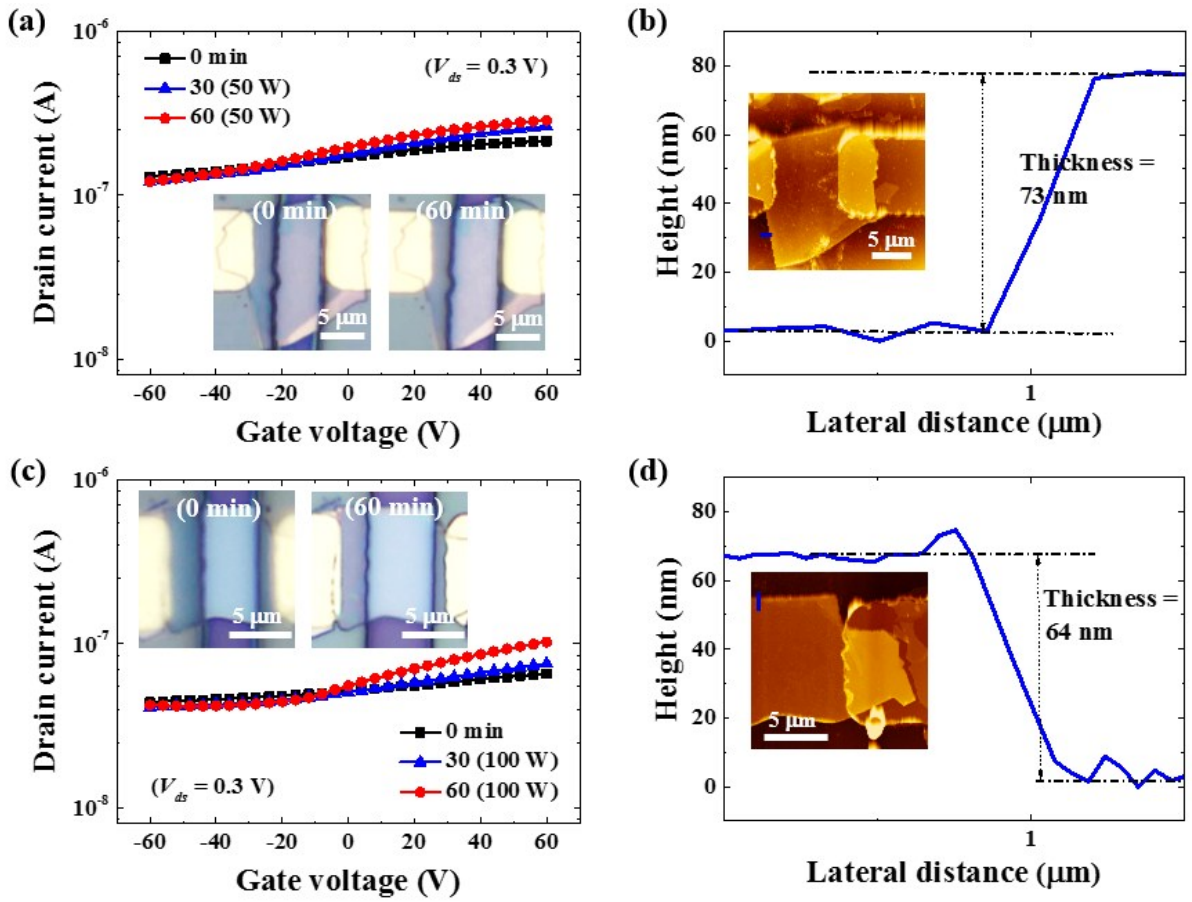

Fig. S5 (a) Transfer characteristics at V_{ds} = 0.3 V for $HfSe_2$ FET with different O_2 plasma exposure times at a power of 50 W, in semi-log scale. The inset shows optical images of $HfSe_2$ FET before and after O_2 plasma treatment for 60 min. (b) Line-profile along the blue line indicates the flake thickness of

~ 73 nm. The inset shows the corresponding AFM image of the $HfSe_2$ FET. (c) Transfer characteristics at V_{ds} = 0.3 V for $HfSe_2$ FET with different O_2 plasma exposure times at a power of 100 W, in semi-log scale. The inset shows optical images of $HfSe_2$ FET before and after O_2 plasma treatment for 60 min. (d) Line-profile along the blue line indicates the flake thickness of ~ 64 nm. The inset shows the corresponding AFM image of the $HfSe_2$ FET.

6. Energy band diagrams for the $HfSe_2$ FET before and after O_2 plasma treatment

The effect of plasma treatment on the $HfSe_2$ FET is illustrated in Fig. S6a and S6b, where the O_2 plasma-induced carrier depletion in the channel resulting in the formation of additional barriers at the interface of photoresist covered and the open channel $HfSe_2$ layers. Therefore, in the plasma-treated device, the injected carriers from the source have to overcome an additional barrier which results in a small decrease in the channel current and a positive shift in the threshold voltage.

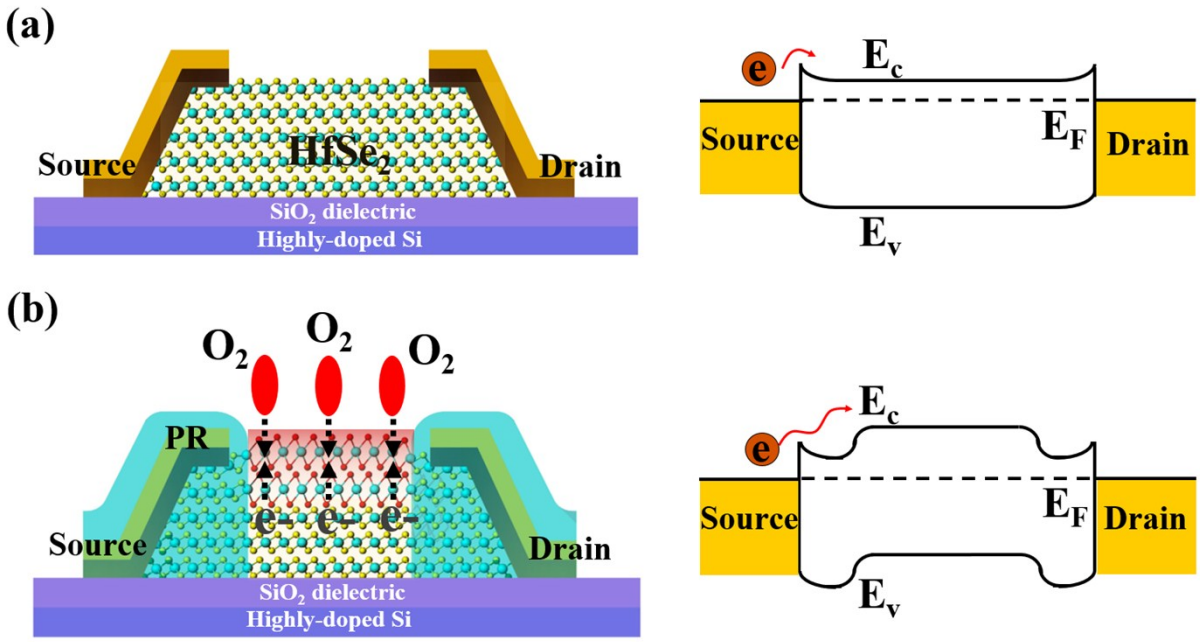

Fig. S6 Schematic energy band diagrams of $HfSe_2$ FET for the conditions of (a) before O_2 plasma treatment and (b) after O_2 plasma treatment.

7. Channel carrier density with O2 plasma-treated time

The plasma treatment is usually followed by the depletion of electron concentration in the channel. Fig. S7 plots the $HfSe_2$ FETs channel carrier density with the plasma-treated time. It can be seen from the figure that after an initial drop, the carrier density stabilizes over a wide range from 5 to 20 min and rapidly decreases thereafter.

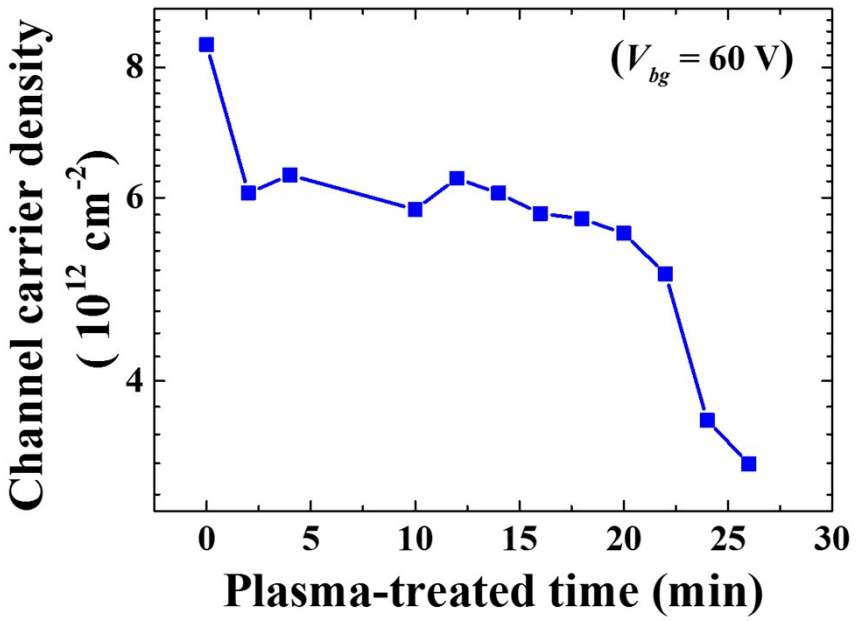

Fig. S7 Channel carrier density of the $HfSe_2$ FETs as a function of the O_2 plasma treatment times.

8. Stability test of the plasma treated and pristine $HfSe_2$ FETs

In order to confirm the effect of the plasma treated top layers on the stability of the devices, we carried out the stability test on both plasma treated and pristine devices. The results illustrate that the off current reduces in both the pristine and plasma devices but the on-current got stabilized in the plasma treated samples, Fig. S8. This can be explained from the passivation effect of the plasma induced oxidized layer, which reduces the rate of oxidation in the plasma treated devices whereas in the pristine device, the absence of top oxidized layers results in higher oxidation rate leading to the reduction in both on and off current of the pristine device. Although the off current decreases in the plasma treated device as well due to the intrinsic time-dependent degradation of the layers thus resulting in the observed decrement in the off current, as shown in the schematic, Fig. S4. However, such intrinsic time-dependent oxidation

would not affect the on current until the layers within the screening length are not affected by the oxidation process.

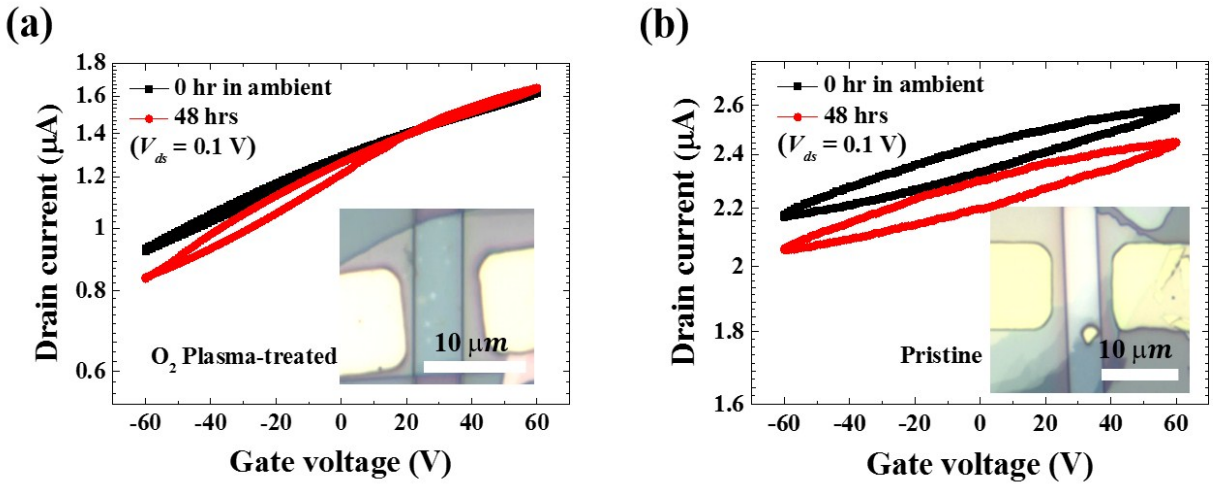

Fig. S8 Transfer measurement of (a) the plasma treated and (b) pristine device over the span of 48 hrs.

9. Photoresponse of pristine and plasma treated $HfSe_2$ photodetector

For a reliable comparison of photoresponse of pristine and plasma treated device and to rule out the flake thickness and ohmic contact variations, we first measure the photoresponse of the pristine device, followed by the plasma treatment of the same device for photoresponse measurement. From the measurement results, the plasma treated device shows better performance as compared to the pristine device, Fig. S9. Important metrics like I_{laser}/I_{dark}, photoresponse time improves with the plasma treatment. The improvement in electrical characteristics and additional defects created by plasma treatment can account for such enhancement as particulary for photoresponse, the creation of additional defects enhaces the recombination rate of the photogenerated carriers, thereby improving the photoresponse time. [S2]

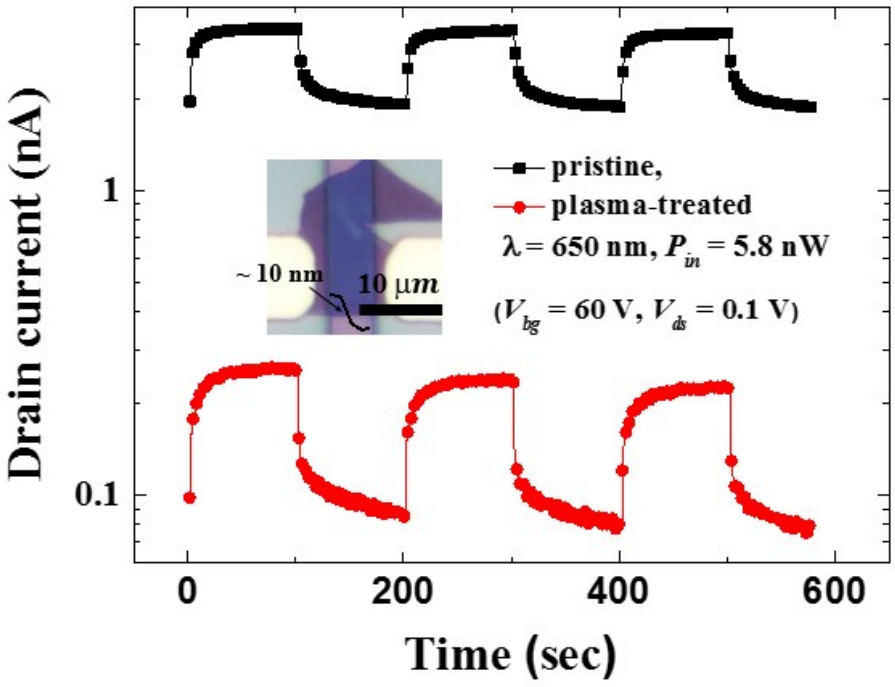

Fig. S9 Temporal photoresponse characteristics of pristine and plasma-treated $HfSe_2$ photodetector, where V_{bg} = 60 V, V_{ds} = 0.1 V. The $HfSe_2$ photodetector treated by O_2 plasma for 10 minute. It was illuminated by laser at wavelength of 650 nm, where the laser incident power was 5.8 nW. The thicknesses of the pristine flake was 10 nm , as measured by atomic force microscopy (AFM).

10. Photoresponsivity and specific detectivity of $HfSe_2$ photodetector at different wavelengths

Fig. S10 shows the calculated photoresponsivity (R) and specific detectivity (D^*) of $HfSe_2$ photodetectors at different wavelengths. Specific detectivity is a measure of detector sensitivity and, assuming that shot noise from dark current is the major contributor to the total noise, it is given by $D^* = RS^{1/2} / (2qI_{dark})^{1/2}$,[S3] where R is the photoresponsivity, S is the active area of the photodetector, q is the unit of charge, and I_{dark} is dark current. Within the wavelength ranging from 520 to 780 nm, the photodetectors show good performance even at the low V_{ds} = 0.1 V. For the visible regions (λ = 520 - 650 nm), R and D^* exist in the range of 0.64 to 2.94 A W^{-1} and 1.01 to 4.65 x 10^{10} Jones, respectively. However, R and D^* of the near-infrared region (λ = 780 nm) are significantly reduced to 48 mA W^{-1} and 7.62 x 10^8 Jones, respectively.

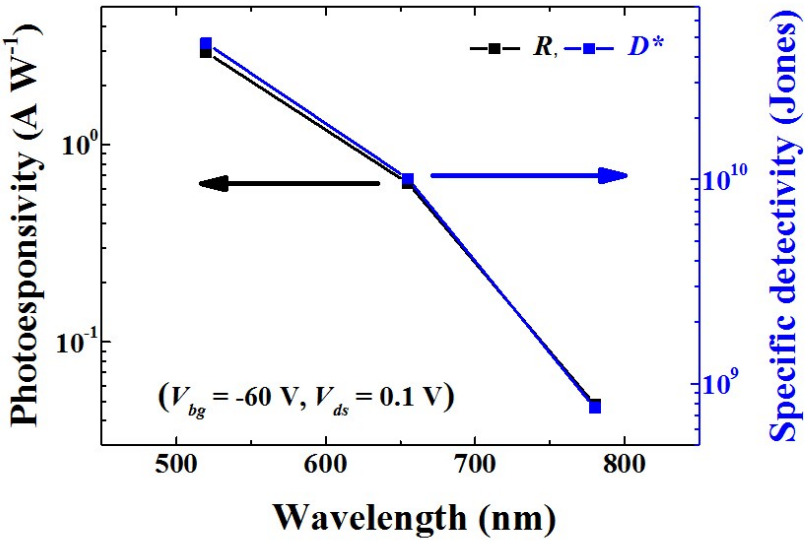

Fig. S10 Photoresponsivity (R) and specific detectivity (D^*) of $HfSe_2$ photodetectors at the different wavelengths.

Supplementary references

S1. Y. Sui and J. Appenzeller, *Nano Lett.*, 2009, **9**, 2973-2977.

S2. J. Shim, A. Oh, D.-H. Kang, S. Oh, S. K. Jang, J. Jeon, M. H. Jeon, M. Kim, C. Choi, J. Lee, S. Lee, G. Y. Yeom, Y. J. Song, J.-H. Park, *Adv. Mater.*, 2016, **28**, 6985-6992.

S3. M. S. Choi, D. Qu, D. Lee, X. Liu, K. Watanabe, T. Taniguchi, W. J. Yoo, *ACS Nano*, 2014, **9**, 9332-9340.